Core−Shell Quantum Dots of Lattice-Matched $ZnCdSe_2$ Shells on InP Cores: Experiment and Theory

Olga I. Micić,*,† Barton B. Smith,*,† and Arthur J. Nozik*,†,‡

National Renewable Energy Laboratory, 1617 Cole Blvd., Golden, Colorado 80401, and Department of Chemistry, University of Colorado, Boulder, Colorado 80309

Received: June 13, 2000; In Final Form: September 22, 2000

Lattice-matched $ZnCdSe_2$ concentric epilayer shells up to 50 Å in thickness have been grown on InP core quantum dots (QDs). The quality of the epitaxially grown shells was monitored by absorption and emission spectra and transmission electron microscopy (TEM). Shell growth was shown to be controllable and was consistently accompanied by a large red shift of the absorption and emission spectra. This results from increased electron delocalization and, hence, lower confinement energy compared to core QDs with no shell. Core−shell nanocrystals also show higher quantum yields for emission since the interface of the QDs is better passivated and deep surface trap luminescence is converted into band-edge luminescence. Theoretical calculations of the electron probability density in these core−shell QDs were made using high-level self-consistent field and tight-binding methods; the theoretical results are consistent with the experimental results.

I. Introduction

Various properties of colloidal semiconductor quantum dots (QDs) can be altered by coating them with a layer or shell of a different semiconductor.[1−19] As initially formed, the surface atoms of QDs are not fully coordinated and are thus highly active for chemical bond formation; this situation invites the possibility for epitaxial overgrowth of another semiconductor. Surface layers can be grown directly on core QDs under conditions where the system is supersaturated with respect to the coating material. Recently, successful chemical syntheses of colloidal core−shell type QDs have been demonstrated; specific systems are (CdSe)ZnS[1,11,12] and the inverse structure,[1] (CdSe)CdS[2,8] and the inverse structure,[8] (CdSe)ZnSe,[13] (CdS)AgS,[4] (CdS)ZnS,[14] (CdS)$Cd(OH)_2$,[5] (CdS)PbS,[10] (HgS)CdS,[7] (Si)SiO_2,[3,15] (InAs)CdSe,[16] (InAs)InP,[16] and CdS/HgS/CdS triple concentric layer structures;[9,17−19] the core material is in parentheses. In such composite QDs, the presence of the shell passivates the core surface and produces strong band-edge photoluminescence (PL).

An important objective in the growth of core−shell structures is to utilize two materials that have nearly the same lattice constants. If core−shell interfaces are not lattice-matched, strain develops during growth which is relieved by the formation of large numbers of dislocations and defects on the core surface; furthermore, the QD core may not be covered homogeneously by the shell, and shell fragments (islands) may form. However, for InP (bulk band gap = 1.35 eV) it is known that strain-free heterostructures can be obtained by deposition of $ZnCdSe_2$ (bulk band gap = 2.2 eV).[20] At $x = 0.475$, $Zn_xCd_{1-x}Se$ has a lattice constant exactly matched to that of InP (5.87 Å); thus, $ZnCdSe_2$ is an ideal shell material for InP QDs. The positions of the conduction band edge (electron affinities) for bulk InP and $ZnCdSe_2$ are 4.4 and 4.0 eV (vs vacuum), respectively, yielding a conduction band offset of about 0.4 eV. Recently, another lattice-matched core−shell system consisting of InAs cores and CdSe shells was reported.[16]

QD cores capped with a second semiconductor layer can change the electronic structure of the QD. The effect is different from that when QDs are coated with organic materials because the semiconductor cap layer provides a well-defined potential barrier that is significantly lower than that of organic barriers; hence, greater penetration of the electron and hole wave functions into the barrier occurs, reducing the degree of quantum confinement.

We report here the synthesis of zinc blende (InP)$ZnCdSe_2$ core−shell QDs. The lattice matching permits epitaxial growth of the $ZnCdSe_2$ shell on colloidal InP QDs; shell thicknesses up to 50 Å were grown on the core InP QDs. The $ZnCdSe_2$ shell causes a shift of the electronic states of the core−shell QDs to lower energy compared to pure InP QDs. Analysis of our results shows that for small core sizes the electron is delocalized over the whole nanocrystal, while the hole is localized mainly within the core. High level theoretical calculations determine the electron probability density of the QDs and are compared with the experimental results.

II. Experimental Section

A. Synthesis of Composite QDs. The core InP QDs, with an average size of 25−45 Å, were synthesized by colloidal chemistry methods using $InCl_3$ and tris(trimethylsilyl)phosphine ($P(SiMe_3)_3$) as starting reactants (molar ratio 1:1). The reactants are heated for 1 day at 270 °C in the presence of trioctylphosphine oxide (TOPO) and trioctylphosphine (TOP). The synthesis is conducted in rigorously air-free and water-free atmospheres. Details of the preparation are given in refs 21 and 22. Fractionation of the QD particles into different sizes was obtained by selective precipitation methods.[23] The QDs were collected as powders and then redispersed in pyridine.

The $CdZnSe_2$ precursor was prepared by mixing dimethylzinc ($ZnMt_2$), dimethylcadmium ($CdMe_2$), and tributylphosphineselenium (TBPSe) in tributylphosphine (TBP) solution in a molar ratio 1:1:4, respectively. Fresh precursor solutions were always prepared before use. Excess Se was used to ensure complete formation of $CdZnSe_2$. Tributylphosphine selenide (TBPSe) was prepared by dissolving Se (1 M) in tributylphosphine (TBP).

We divided the InP QD solution into multiple fraction in order to have a series of samples with the same InP core but different

† National Renewable Energy Laboratory.
‡ University of Colorado.

10.1021/jp0021502 CCC: $19.00
Published on Web 11/18/2000

shell thicknesses. A sample containing 2−8 mg of InP QDs was dispersed in pyridine. In the next step, InP was overcoated with $CdZnSe_2$ in pyridine at 100 °C. Successful overcoating of QDs in pyridine at 100 °C has been previously used for (CdSe)-CdS QDs.[2] We calculated the ratio of the $ZnCdSe_2$ precursor to InP necessary to form a shell of a desired thickness based on the ratio of the volume of the shell to that of the core assuming that spherical cores and annular shells are formed. The precursor solution was diluted (concentration of Zn and Cd was 0.01 M) inside an inert atmosphere glovebox. The $CdZnSe_2$ precursor was loaded into a syringe and then 1−5 mL was added dropwise to the reaction solution at 100 °C. The solution becomes darker as the precursor for the overcoat was added. Oleylamine (*cis*-1-aminooctadecene) was added to the reaction solution at room temperature and pumped off; the QDs were then redissolved in hexane. The actual amount of $CdZnSe_2$ that grows onto the InP cores was generally less than the amount added due to incomplete reaction of the precursor. Small bare $ZnCdSe_2$ particles that also formed to a small extent were removed by centrifugation and precipitated with methanol. Finally, the core−shell nanocrystals were redissolved in hexane and filtered through a 0.2 μm filter.

B. Optical Characterization. Optical absorption spectra were collected at room temperature using a Cary 5E UV−vis−near-IR spectrophotometer. PL spectra were obtained at room temperature using an SPEX Fluorolog-2 spectrometer. Luminescence quantum yields for QD solids and solutions were measured relative to the known luminescence intensities of organic dyes.

C. Transmission Electron Microscopy. A Phillips CM-30 electron microscope operating at 200 kV was used for transmission electron microscopy (TEM). Imaging was carried out in bright field with an objective aperture selected to permit lattice imaging of the ⟨111⟩ zinc blende plane. The samples were prepared by placing 2.5 μL of a dispersion of QDs in a mixture of octane(0.9)/octanol(0.1) directly onto a copper grid supporting a thin film of amorphous carbon and allowing it to slowly evaporate. For EDAX measurements (energy-dispersive X-ray analysis) the QD solution was evaporated on a carbon grid to a depth of about 0.1 μm. EDAX intensities were calibrated by examination of commercial bulk powders of $ZnCdSe_2$ and InP.

III. Results and Discussion

A. Experimental. *1. Synthesis of Core−Shell Structures.* $ZnCdSe_2$ grows onto the InP core making larger nanocrystallites with a core−shell structure. In the first step, InP QDs were synthesized with diameters in the range of 20−45 Å, with a final size distribution of about 10%. These QDs are initially passivated with TOP/TOPO capping groups which are then replaced with pyridine before the addition of the $ZnCdSe_2$ shell. In the second step the $ZnCdSe_2$ precursor was used to overcoat InP QDs in pyridine at 100 °C. This low-temperature procedure is the same as that used by Peng et al.[2] for overcoating CdSe with CdS. Shell growth was completed immediately after addition of the $ZnCdSe_2$ precursor in pyridine solution at 100 °C. The growth of the $ZnCdSe_2$ shell was monitored by optical absorption, PL spectra, and TEM.

In the synthesis of (InP)$ZnCdSe_2$ QD samples, we also found that extremely small bare $ZnCdSe_2$ particles, which have an absorption peak at 370 nm, were also formed, and that they are only slightly soluble in pyridine. Because of that, they could be easily separated by selective precipitation methods while the core−shell QDs were retained. The formation of the bare $ZnCdSe_2$ particles can be minimized by choosing appropriate conditions during the overcoating procedure, such as very slow addition of diluted solutions of $ZnCdSe_2$ precursor to diluted InP QD solutions, and immediately stopping heating after addition of precursor.

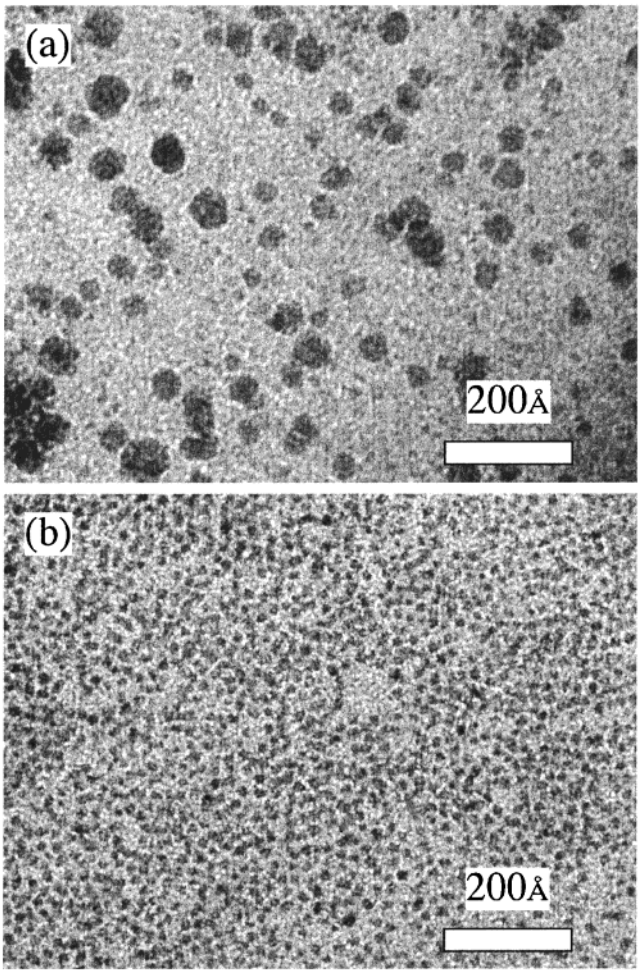

Figure 1. TEM image of (InP)$ZnCdSe_2$ QDs with 30 Å InP core: (a) after and (b) before coating with the $ZnCdSe_2$ shell. Coated QDs are in the range 50−100 Å and are well dispersed and not agglomerated.

The final shell thickness is not intrinsically limited since the shell grows with no lattice strain. Figure 1 shows TEM images of (InP)$ZnCdSe_2$ core−shell QDs (Figure 1a) that were prepared by overcoating 30 Å InP core QDs (Figure 1b). (InP)$ZnCdSe_2$ QDs are isolated prolate particles that have diameters ranging between 50 and 100 Å; we estimate an average diameter to be 70 Å ± 30%. Figure 2 shows high-resolution TEM of a bare InP QD and the subsequently formed core−shell (InP)$ZnCdSe_2$ QD; the QDs show well-resolved ⟨111⟩ lattice fringes in particles that have the proper orientation for observation of fringes. Lattice fringes that extend throughout the particles (Figure 2, right panel) showed that the growth of the $ZnCdSe_2$ shell is epitaxial. Core−shell QDs have a zinc blende structure and a measured lattice spacing (3.4 Å) that is the same as that in the bare InP QDs. Differences in lattice constants between the core and shell are very small even when the Zn/Cd ratio in the shell changes from 0.5 to 1.5. In that case, the length of the Zn−Se (or Cd−Se) bond in $ZnCdSe_2$ differs by less than 2% of the In−P bond distance. The definition of a monolayer here is a $ZnCdSe_2$ shell that measures 5 Å, which is double the length of the In−P bond in the crystal lattice of InP. We observed shell growth up to 10 monolayers (50 Å).

We found that large core−shell QDs (diameter 70−200 Å) are also very well dispersed in nonpolar solvents (hexane,

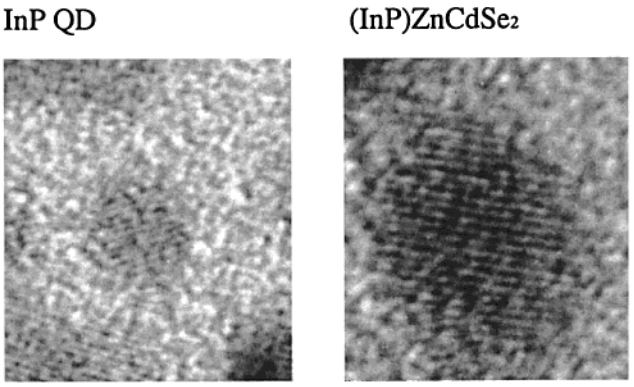

Figure 2. High-resolution TEM image showing lattice fringes of QD oriented with the ⟨111⟩ axis in the plane of the micrograph. Interplanar spacing for ⟨111⟩ is 3.4 Å, which is the same as bulk InP. The left panel shows an InP QD before capping and the right panel shows a core−shell (InP) ZnCdSe QD after capping.

toluene, chloroform) because the core−shell QDs are capped with oleylamine, which keeps them dispersed in solution. This capping group was present on all QDs in our samples.

EDAX analysis shows that the InP QDs are typically prepared with In/P ratios of approximately 1.1−1.0. To check the possible error in the P atom content that originated from TOPO/TOP that remained on the QD surface even after replacement with the oleylamine stabilizer, we synthesized InP QDs in trioctylamine solution at 265 °C; we found the same ratio of In/P as that in QDs synthesized with TOPO/TOP. InP QDs are prepared with a slight shortage of phosphorus. EDAX indicated a Cd/Zn ratio in (InP)$ZnCdSe_2$ powder close to 1, while the Cd/Se ratio is about 0.5−0.4. Powders of core−shell QDs also show a negligible presence of Cl, O, and C. On the other hand, EDAX results for the Zn/In ratio are less than those calculated from the $ZnCdSe_2$ precursor concentration; this indicates that bare $ZnCdSe_2$ particles are also formed.

2. Absorption and PL Spectra. Figure 3, a and b, shows optical absorption spectra for QDs having two different core sizes of 22 and 42 Å, respectively, and approximately the same shell thickness (5 Å, one monolayer). The QD absorption spectra are characteristic of InP QDs (δ = 10%) with an absorption onset significantly shifted from that in bulk InP (E_g = 1.35 eV; 916 nm) due to the quantum confinement. During shell growth the absorption features are broadened, and at same time shifts to lower energy. We observed a red shift (lower energies) of 50 meV in the absorption spectrum of smaller cores of 22 Å after overcoating them with 5 Å $ZnCdSe_2$ (Figure 3a); a smaller red shift of 10 meV was observed for a larger core of 42 Å InP QDs (Figure 3b). In smaller QDs the leakage of the electron and hole wave functions into the neighboring $ZnCdSe_2$ shell has a more dramatic effect on the confinement energies of the charge carriers.

The evolution of the PL spectra for 22 and 42 Å InP QDs with the same coverage of $ZnCdSe_2$ (5 Å) is displayed in Figure 4, a and b, respectively. Uncapped core QDs for both sizes showed no detectable bandedge emission. After etching colloidal QD solutions with HF, we determined the position of the PL peak for bare 22 Å InP QDs to be 580 nm, and for 42 Å to be 670 nm. We showed previously that controlled etching of InP QDs suppresses trap emission and enhances bandedge emission.[24] We chose samples with very weak initial band edge emission in order to see the ability of $ZnCdSe_2$ to electronically passivate InP QD surfaces. Upon capping InP QDs with $ZnCdSe_2$, we observed a dramatic increase in the intensity of band edge emission. We found that the luminescence quantum

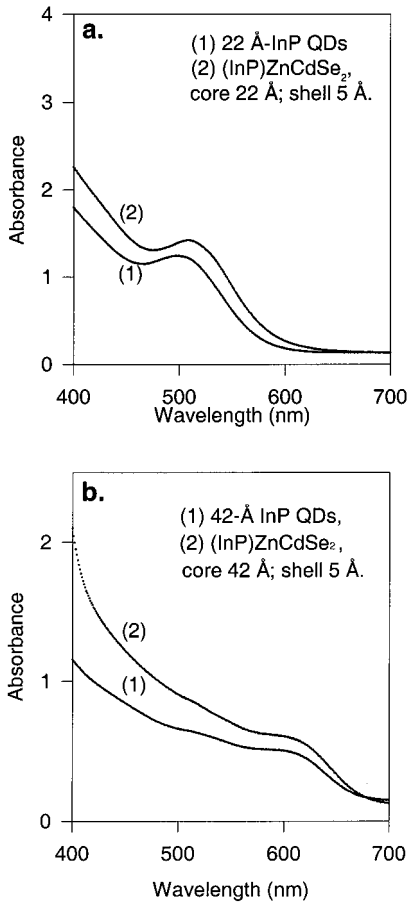

Figure 3. Room temperature absorption spectra of (InP)$ZnCdSe_2$ QDs with 22 and 42 Å core diameters and 5 Å shell thickness.

yields are 5−10% for samples with 5 Å $ZnCdSe_2$ caps. We also found that QD samples that were first etched with HF and then overcoated with $ZnCdSe_2$ show poor core−shell structure. It appears that HF blocks the surface and does not allow epitaxial growth of the $ZnCdSe_2$ layer.

(InP)$ZnCdSe_2$ QDs are more stable to surface oxidation, which can be an advantage since bare InP is very sensitive to surface oxidation. A major characteristic of InP QDs is that after synthesis both In and P atoms on the surface oxidize easily upon exposure to air, and a surface oxide layer is formed.[24−26] This also occurs with bulk InP where undefined oxide layers are formed (In_2O_3, $In(OH)_3$ P_2O_3, $InPO_4$, $In(PO_3)$).[27] The stability of core and core−shell nanocrystals was compared when samples were exposed to light irradiation in the presence of oxygen. The bare InP core samples showed a washing out of optical absorption features, while core−shell QDs showed little change. This has been noticed previously for different core−shell structures, and has been explained by hole confinement in the core, which decreases the anodic corrosion on the surface.[12]

3. Shell Growth Effect. We focus our attention on the evolution of the optical spectra as a function of the $ZnCdSe_2$ coverage for one particular size of the InP core. Bare InP QDs with a diameter of 30 Å were overcoated with $ZnCdSe_2$ shells of approximately 15, 23, 32, and 50 Å thickness. Figure 5a shows the absorption spectra as a function of shell thickness; the overall shape is roughly constant, but there is a slight broadening of features, which shift to lower energy with increased shell thickness. The red shift is approximately 30 meV per one layer of $ZnCdSe_2$ coverage (10 Å increase in diameter).

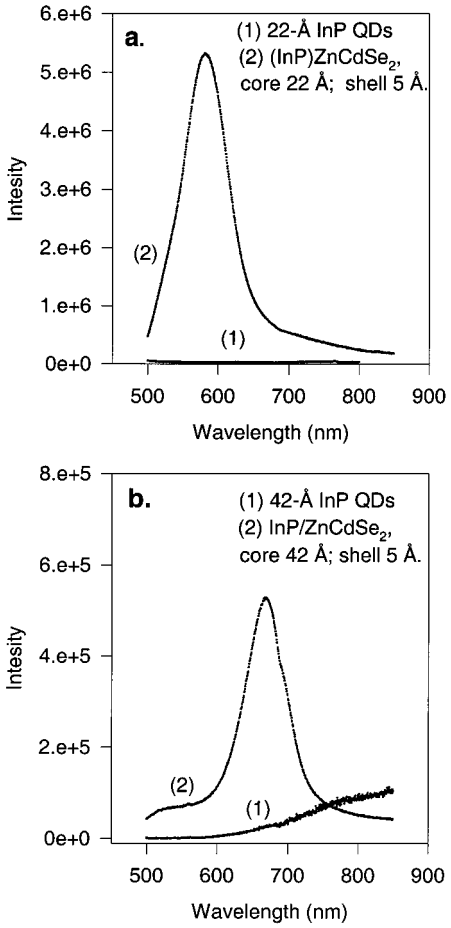

Figure 4. Room temperature PL spectra of (InP)$ZnCdSe_2$ QDs with 22 and 42 Å core diameters and 5 Å shell thickness. The uncapped core nanocrystals gave no detectable bandedge luminescence; the positions of the band edge emission peaks of HF-etched bare 22 and 42 Å InP QDs (ref 24) are at 580 and 670 nm, respectively.

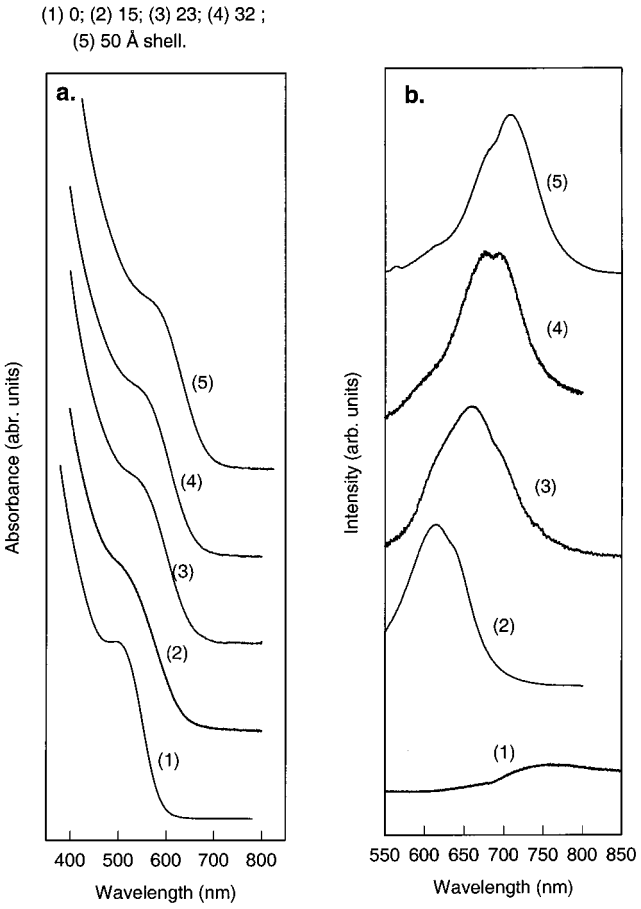

Figure 5. Room temperature absorption (a) and PL (b) spectra of a series of core−shell QDs consisting of InP cores 30 Å in diameter and $ZnCdSe_2$ shells varying from 0 to 50 Å in thickness.

This change in absorption spectra is caused by the decrease in electronic level separation as the shell size increases.

A pronounced red shift has also been recently reported for 34 Å InAs QDs overcoated with either CdSe or InP shells.[16] In the latter case, a decrease of PL efficiency was observed, while in the former case the PL efficiency increased. The enhanced PL is similar to our result for (InP)$ZnCdSe_2$ QDs and is attributed to the better quality surfaces for the II−VI materials compared to InP surfaces.[16]

A red shift was also obtained for the PL spectra. The evolution of the PL spectra with increasing shell coverage for the same 30 Å diameter core is shown in Figure 5b. As the thickness of the $ZnCdSe_2$ shell increases, the spectra red shift, similar to the red shifts in the absorption spectra. Uncapped core InP QDs for both sizes gave no detectable band edge emission.

In small core−shell (InP)$ZnCdSe_2$ QDs the electronic wave function extends out from the core into the shell; this reduces the confinement energy and produces a red shift in the absorption and emission spectra compared to the core itself. In Figure 6 the difference in energy (red shift) for the PL peaks between core InP QDs (30 Å diameter, emission maximum at 602 nm) and 30 Å QDs with a $ZnCdSe_2$ shell of various thicknesses is presented (filled circles). Also shown is the difference in the PL peak for a 30 Å InP QD and InP QDs consisting of the 30 Å core plus an additional InP shell of various thicknesses (open circles). Thus, for example, the open circle data point for the InP QD with a shell thickness of 25 Å represents an InP QD with a total diameter of 80 Å (30 Å + (2 × 25 Å)).

The red shift in emission for the 30 Å InP core and 25 Å $ZnCdSe_2$ shell is about 180 meV; this shift is much smaller than that (535 meV) for the QD with a 30 Å InP core and a 25 Å InP shell (i.e., an 80 Å diameter InP QD). This is to be expected (see discussion of theoretical calculations below) since the delocalization or spreading of the wave function in the core−shell QD through penetration of the barrier region is not as extensive as the delocalization for core-only InP QDs of equivalent total diameter.

Since the core−shell QDs also have an organic cap, which has a large effective band gap, the actual potential energy diagram for the system consists of a quantum well with a stepped potential barrier. The first barrier is the shell and the second barrier is the organic cap. The resulting quantized levels for electrons and holes will depend on the core diameter, the thicknesses of the $ZnCdSe_2$ shell and organic cap, and the electron affinities and band gaps of the core, shell, and organic cap materials.

B. Theory. *1. Theoretical Methods.* High-level theoretical calculations of the (InP)$ZnCdSe_2$ core−shell QDs were performed in order to obtain quantitative insight into the origin of the red shift between the absorption and emission spectra of a core InP QD and a core−shell QD containing the same InP core with a $ZnCdSe_2$ shell. The high-level methods that were used are density functional (DFT) calculations in the LDA and B3LYP forms[28,29] and ab initio HF calculations using the LACVP** basis set. However, because of practical limitations on CRAY time, these highest level calculations were only

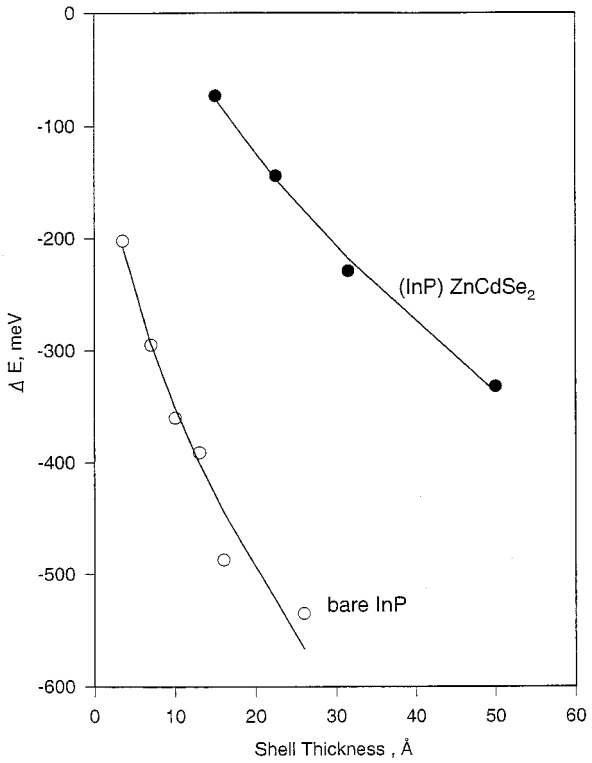

Figure 6. Filled circles: red shift vs $ZnCdSe_2$ shell thickness for a (InP)$ZnCdSe_2$ core−shell QD with a 30 Å diameter InP core. Open circles: red shift vs shell thickness for pure InP QDs defined as the shift between a 30 Å InP core and larger InP QDs where the shell thickness is defined as the thickness of the additional InP shell added to the 30 Å InP core.

performed on small QDs of less than 60 semiconductor atoms (maximum QD diameter of about 14 Å). Both the PS-GVB and Gaussian 98 codes were used to implement the DFT techniques.[30,31] The LACVP** calculations were performed with PS-GVB.[31] One of the approaches we employed for QDs larger than 14 Å in diameter (we focus on spherical dots below) was the PM3 semiempirical method of MOPAC.[32] The DFT and HF results were used to reparametrize the PM3 Hamiltonian[32] in order to match the higher level results as closely as possible. We used a 6 and 10 Å cutoff for the overlap and two electron PM3 integrals, respectively.

All theoretical studies of large QDs must trade rigor and accuracy for gains in computational speed. The minimum core diameter of QDs studied here experimentally was 22 Å, and hence are larger than the QD diameters that could be addressed using the highest level theoretical methods. However, as usual, it was important to perform these calculations, since the lower level calculations which must be used with larger dots have a number of deficiencies. Indeed, many of the parameters in the lower level methods can only be obtained from higher level calculations like those we employed, or from experimental data. The PM3 atomic parameters are the same for surface and interior atoms and, ideally (at least by definition), are insensitive to different bonding environments. The main question that remains is if the latter is actually true, i.e., is the parametrization and Hamiltonian sufficiently universal so that it can address atoms in different bonding environments and thus accurately describe dots of various sizes and structures which have different crystal face, surface, and sometimes global geometry (e.g., departures from perfect spherical shape due to atomic discreteness). This question will not have a definite answer for any simplified electronic method used for QDs, until improved experimental and/or computational abilities are realized. (Of course, even very low level methods are capable of reproducing the main characteristics of QDs.) Since PM3 is a self-consistent method, as we next discuss, it has a much greater chance of being universal than the typical non-self-consistent methods that are employed for QDs.

We note that PM3 is a self-consistent field (SCF) approach. Non-self-consistent methods are typically employed for QDs (e.g., effective mass approximation, empirical pseudopotential method, tight-binding approaches). The important effects of self-consistent electron density redistribution are typically not addressed at all with the latter methods, and when they are, considerable ad hoc reparametrization is usually necessary. Here, use of a SCF method is especially important because the two materials (core and shell) have significant electronic reorganization as a result of formation of the interface. However, we also employed a tight-binding (TB) method (the extended Huckel methodology)[33,34] for more qualitative insight when examining QDs larger than could be addressed with DFT or PM3. We used different tight-binding parameters for atoms at the interface between core and shell to match our PM3 results for smaller QDs as closely as possible, with the assumption that the TB reparametrization will hold for larger QDs. Dots with 20 Å cores were examined with TB, and an abbreviated test study of a dot with a 17 Å core was performed with PM3 (only a core−shell dot was examined with a 4 Å shell). The results from these TB and PM3 studies were qualitatively the same as we report below for a smaller dot. A more systematic study of effects of dot structure and size, and comparisons of theoretical methodologies, are reserved for a separate paper.

While our PM3 method is inherently more appropriate for core−shell systems than non-self-consistent methods, we have not yet fully optimized our PM3 reparametrization. Our reparametrization gave reasonable matches to the results of our higher level methods, but some of the band structure is in need of improvement. The model should be sufficiently accurate for the questions we pose here, and it addresses surface and interface effects much more accurately than non-self-consistent methods. Even highly sophisticated methods have difficulty accurately reproducing band gap energies. We discuss the accuracy of our results below. It is more difficult to fully passivate the system when SCF methods are used, versus non-self-consistent approaches, since the SCF method has a realistic description of the surface. Thus, our calculations sometimes showed surface states in the gap, even though we used hydrogen-like atoms to passivate surface dangling bonds. In the real-world system, the QD surface may be significantly reconstructed and this may eliminate or significantly reduce gap surface states; the organic capping materials may also play a significant role. In our idealized model, we simply cut QDs out of bulk materials and passivated the resulting dangling bonds with the artificial hydrogen-like atoms—a typical technique.[35] Only vacuum is present outside of our idealized QDs.

2. Results. We examined QDs of spherical and cubic shape. The results were similar, and we report here only on the former. A number of spherical QD sizes were examined. Here, we focus on one core−shell QD size, which corresponds to a total atomic center to center diameter of 19 Å, excluding passivating atoms that are included in the calculation to take care of surface dangling bonds. We will denote this as the 19 Å diameter QD; the InP core is just under 12 Å (atomic center to atomic center), and the $ZnCdSe_2$ shell thickness is about 3.5 Å.

The characteristics of the QD band edge states are of most interest, since they can be used to predict the experimental red shift between core and core−shell QDs. It will prove instructive

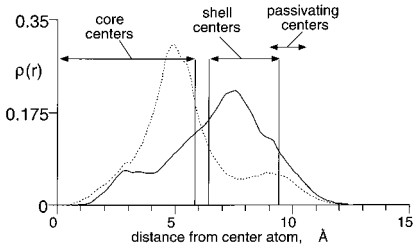

Figure 7. PM3-calculated radial electron probability density ($\rho(r)$) for a (InP)$ZnCdSe_2$ QD with a total atomic center to center diameter of 19 Å excluding the passivating atoms). The dashed line shows the $\rho(r)$ for the VB maximum (HOMO), the solid line for the CB band minimum (LUMO) states. The positions of the shell, core, and passivating atomic centers are indicated.

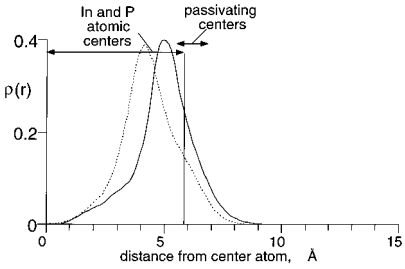

Figure 8. Same as Figure 7 except the $\rho(r)$ for the InP core of the core−shell QD of Figure 7 is plotted. The PM3 method was used; the VB maximum state $\rho(r)$ is dashed and the CB minimum state $\rho(r)$ is solid. Positions of atomic centers are indicated.

to plot the radial probability density (a quantity receiving copious use in atomic quantum physics and chemistry)[36] for these states. To find this density we first calculated the probability of finding an electron (in a given state) in a thin spherical shell a distance r from the center of the QD. To find this probability, we multiplied the probability density (the full three-dimensional probability density $|\Psi|^2$) for a given volume element within the shell by the volume of the element. We then summed these results for all the volume elements in a given shell, giving the probability of finding an electron in that shell. In turn this is converted into the radial probability density $\rho(r)$ (with dimensions length^{-1}) by simply dividing by the thickness (Δr) of each shell. It is this $\rho(r)$ that we plot here. We note the numerical technique used to find $\rho(r)$ was actually more complicated than described. To correct the geometrical mismatch of cubic boxes (used in the electronic structure calculation) with the spherical shell edges, we wrote an averaging and interpolation algorithm, and also employed Simpson's rule for the quadrature.

Figures 7 and 8 compare the radial probability density for the valence band (VB) maximum state (HOMO) (dashed lines) and the conduction band (CB) minimum state (LUMO) (solid lines) of the 19 Å diameter core−shell (InP)$ZnCdSe_2$ QD (Figure 7) with that of the pure InP core QD (in a vacuum and terminated with hydrogen-like atoms) (Figure 8) (some of these states are degenerate). For these plots the PM3 method was used; results for the TB method were qualitatively the same, but for the TB model the spatial resolution of the probability density, of course, can only be performed crudely. In Figures 7 and 8 the results for each edge state (CB and VB) are normalized to 1; $\rho(r)$ approaches zero at $r = 0$, since the shell volumes approach zero. Figure 9 shows the $\rho(r)$ for both band edge states for a pure InP QD with the same total diameter (19 Å) as the core−shell QD. We also employed both PM3 and the TB method for this size QD, and the PM3 results are plotted in Figure 9.

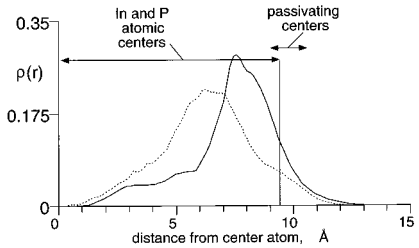

Figure 9. This figure is the same as Figure 7 except it plots $\rho(r)$ for a pure 19 Å InP QD. Again, the PM3 method was used and the VB maximum state $\rho(r)$ is dashed and CB minimum state $\rho(r)$ is solid. Positions of atomic centers are indicated.

Figures 7−9 show that the penetration of the radial probability density to the surface is greater for the pure 19 Å InP QD (Figure 9) compared to the core−shell QD with the same total diameter (Figure 7), particularly for the VB minimum state. We see in all the cases we examined with all our methods that for near band edge states the wave function, standard probability density, and radial probability density exhibit greater spatial extent in pure InP QDs compared to (InP)$ZnCdSe_2$ core−shell QDs of equivalent diameter. If one compares Figures 7−9, it is obvious that adding an InP shell (Figure 9) to the InP core of Figure 8 will result in more probability density spreading out into the shell region than if a $ZnCdSe_2$ shell (of equal thickness) is added (Figure 7). Thus, reasoning from a particle in a box perspective, one would expect that the red shifts (relative to a fixed core size) of the optical transitions for pure InP QDs as a function of shell thickness compared to a core−shell QD (with the same InP core diameter) would be larger for the pure QDs than the (InP)$ZnCdSe_2$ QDs. This is consistent with the experiments reported above (Figure 6) and the results of the calculations we present next. Some qualifications to this picture are discussed at this section's end.

The PM3 results for the (InP)$ZnCdSe_2$ QD of Figure 7 show a predicted red shift relative to the InP core alone for band gap absorption or emission of about 160 meV. This is the difference between the band gaps of the passivated 12 Å InP core and the full 19 Å (InP)$ZnCdSe_2$ QD. The band gaps are defined as the difference between the calculated valence band maximum and conduction band minimum eigenvalues. The pure InP QD of Figure 9 shows a predicted absorption red shift of about 500 meV (i.e., the difference of the band gaps of the passivated 12 Å pure InP core QD and the 19 Å pure InP QD). The theoretically calculated red shift for the (InP)$ZnCdSe_2$ QD is larger than the experimental results closest to this QD size (see Figure 6); this is expected since the theoretical InP core is smaller than in the experiments, while the shell is roughly the same size. However, the error in the PM3-calculated band gaps for the 19 Å QD versus the real world may be as large as ± 0.3 eV, even after standard[35,37] electron−hole Coulomb corrections are added (the correction is about 0.2 eV for InP for this QD size). This latter correction is omitted in our red shift calculations (the difference for a 12 Å versus a 19 Å InP QD is about 0.1 eV). The band gap error of the electronic structure calculations themselves may actually cancel to some degree in the red shift calculation. In any event, the results are in qualitative agreement with experiment, and this seems rather insensitive to atomic parameter changes. The tight-binding calculations are currently not sufficiently well parametrized to give absolute quantitative results for the red shift, but they are also in qualitative agreement with experiment.

Figure 10 shows the conduction band minimum electron probability density isosurfaces for the core−shell QD of Figure 7. The top panel shows a slice through the center of the QD

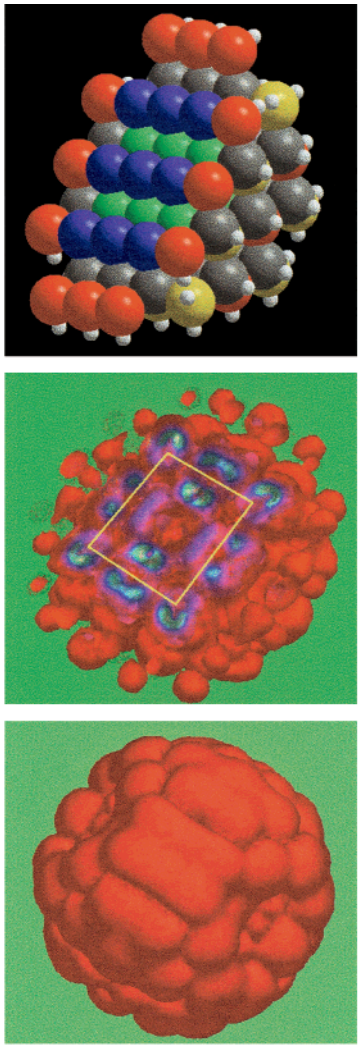

Figure 10. (Top panel) Hard-sphere representation of the atomic structure of the (InP)$ZnCdSe_2$ QD of Figure 7 shown with a slice through the QD center perpendicular to the [001] direction. Green = P, blue = In, red = Cd, yellow = Zn, and gray = Se. (Middle panel) Three-dimensional electron probability density isosurfaces (portrayed as weakly translucent) for the QD shown in the top panel with the same orientation and slice through the middle of the QD. The yellow rectangle at the QD center outlines the outermost positions of the centers of the core InP atoms. (Bottom panel) A single 3-dimensional electron probability density isosurface (portrayed as opaque) for the full dot (not sliced). This low magnitude density outlines the surface, and one can see various crystal faces only slightly masked by passivator atom density.

with the QD atoms represented as spheres. The middle panel shows the electron probability density of the sliced QD with the same orientation as the top panel. The bottom panel shows the full 3-D representation of the electron probability density of the QD (not sliced) with only a low-density isosurface shown. The density outlines the surface—one can see various crystal faces only slightly masked by the passivating atoms. While the plots of radial probability density in Figures 7−9 are instructive, obviously they do not reflect the rich electronic structure of this system as indicated in Figure 10. A great deal of smoothing occurs in the summations used to calculate the radial probability density. The system has other complexities.

While a simple particle in a box outlook is consistent with the results, it may prove worthwhile to investigate the system further by allowing for reconstructed surfaces and even including a model of the organic capping layer. However, the band edge states themselves do not have significant surface character, as Figures 7−9 show, i.e., most of the density is not surface density. Thus, the red shift may well be rather insensitive to surface effects.

Finally, we note that a very common approach to core/shell systems is based on the effective mass approximation (EMA). The qualitative picture that emerges from EMA shows a competition between kinetic energy and potential energy (in the effective mass Hamiltonian), which results in a number of interesting system-dependent phenomena.[6,37] In our case, the electron effective mass is larger in the shell than in the core for the (InP)$ZnCdSe_2$ QD. For certain core and shell sizes, EMA shows the kinetic energy of the electrons will be greater than the potential well in the core. EMA would predict that the electron density will thus tend to shift into the shell as a result of this effect to lower the kinetic energy. We see some evidence for this effect in our system, especially in our TB results. But the scope of our study, especially in our range of QD sizes and shapes, was not large enough to fully explore it. The hole masses in the core and shell are roughly the same, and the gain or loss of kinetic energy by shifts to core or shell will be less significant.

IV. Conclusion

Core−shell quantum dots with a zinc blende structure consisting of InP cores and lattice-matched $ZnCdSe_2$ shells have been successfully prepared by colloidal chemistry. HRTEM images of the QDs show well-resolved lattice fringes that extend through the whole QD crystal, indicating lattice-matched epitaxial growth of the shell onto the core. The $ZnCdSe_2$ shell passivates the surface of the InP core. Hence, bare InP cores with diameters of 22 and 42 Å exhibited no photoluminescence, while these cores capped with a 5 Å $ZnCdSe_2$ shell show PL quantum yields of 5−10% at room temperature. The absorption and emission spectra show a red shift of the core−shell QD compared to the core alone. The red shift was measured as a function of $ZnCdSe_2$ shell thickness (up to 50 Å) for a core diameter of 30 Å, and increased with increasing shell thickness. This red shift was not as large as that between a 30 Å InP core and a larger InP QD consisting of the 30 Å InP core plus InP shells of equivalent thickness to the (InP)$ZnCdSe_2$ QDs. High-level calculations of the electronic structure of the core−shell (InP)$ZnCdSe_2$ and bare InP QDs were made using both self-consistent field and tight-binding methods. The wave functions and electron radial probability density distributions were calculated, and the former produced theoretical red shifts that were consistent with experiment. The lower-level tight-binding calculations yielded results that were qualitatively similar to the higher level approaches.

Note Added in Proof. A new manuscript on core-shell QDS has appeared after this manuscript was accepted (Y. W. Cao and U. Banin, *J. Am. Chem. Soc.* **2000**, *122*, 9692).

Acknowledgment. This work was supported by the U.S. Department of Energy, Office of Science, Office of Basic Energy Sciences, Division of Chemical Sciences, Geosciences, and Biosciences. We are indebted to Phil Ahrenkiel for the high-resolution TEM images of the quantum dots. O.I.M. thanks Andrew Williamson for very helpful discussions.

References and Notes

(1) Kortan, A. R.; Hull, R.; Opila, R. L.; Bawendi, M. G.; Steigerwald, M. L.; Carroll, P. J.; Brus, L. E. *J. Am. Chem. Soc.* **1990**, *112*, 1327.

(2) Peng, X.; Schlamp, M. C.; Kadavanich, A. V.; Alivisatos, A. P. *J. Am. Chem. Soc.* **1997**, *119*, 7019.

(3) Wilson, W. L.; Szajowski, P. F.; Brus, L. E. *Science* **1993**, *262*, 1244.

(4) Spanhel, L.; Weller, H.; Fojtik, A.; Henglein, A. *Ber. Bunsen-Ges. Phys. Chem.* **1987**, *91*, 88.

(5) Spanhel, L.; Haase, M.; Weller, H.; Henglein, A. *J. Am. Chem. Soc.* **1987**, *109*, 5649.

(6) Haus, J. W.; Zhou, H. S.; Honma, I.; Komiyama, H. *Phys. Rev. B* **1993**, *47*, 1359.

(7) Hasselbarth, A.; Eychmueller, A.; Eichberger, R.; Giersig, M.; Mews, A.; Weller, H. *J. Phys. Chem.* **1993**, *97*, 5333.

(8) Tian, Y.; Newton, T.; Kotov, N. A.; Guldi, D. M.; Fendler, J. H. *J. Phys. Chem.* **1996**, *100*, 8927.

(9) Mews, A.; Kadavanich, A. V.; Banin, U.; Alivisatos, A. P. *Phys. Rev. B* **1996**, *53*, R13242.

(10) Zhou, H. S.; Honma, I.; Komiyama, H.; Haus, J. W. *J. Phys. Chem.* **1993**, *97*, 895.

(11) Hines, M. A.; Guyot-Sionnest, P. *J. Phys. Chem. B* **1996**, *100*, 468.

(12) Dabbousi, B. O.; Viejo, J.; Mikulec, F. V.; Heine, J. R.; Mattousi, H.; Ober, R.; Jensen, K. F.; Bawendi, M. D. *J. Phys. Chem. B* **1997**, *101*, 9463.

(13) Danek, M.; Jensen, K. F.; Murray, C. B.; Bawendi, M. G. *Chem. Mater.* **1996**, *8*, 173.

(14) Youn, H. C.; Baral, S.; Fendler, J. H. *J. Phys. Chem.* **1988**, *92*, 6320.

(15) Littau, K. A.; Szajowski, P. J.; Muller, A. J.; Kortan, A. R.; Brus, L. E. *J. Phys. Chem.* **1993**, *97*, 1224.

(16) Cao, Y.-W.; Banin, U. *Angew. Chem., Int. Ed. Engl.* **1999**, *38*, 3692.

(17) Schooss, D.; Mews, A.; Eychmoeller, A.; Weller, H. *Phys. Rev. B* **1994**, *49*, 17072.

(18) Eychmueller, A.; Vossmeyer, T.; Mews, A.; Weller, H. *J. Lumin.* **1994**, *58*, 223.

(19) Mews, A.; Eychmueller, A.; Giersig, M.; Schooss, D.; Weller, H. *J. Phys. Chem.* **1994**, *98*, 934.

(20) Dai, N.; Cavus, A.; Dzakpasu, R.; Tamargo, M. C.; Semendy, F.; Bambha, N.; Hwang, D. M.; Chen, C. Y. *Appl. Phys. Lett.* **1995**, *66*, 2742.

(21) Mićić, O. I.; Curtis, C. J.; Jones, K. M.; Sprague, J. R.; Nozik, A. J. *J. Phys. Chem.* **1994**, *98*, 4966.

(22) Mićić, O. I.; Sprague, J. R.; Curtis, C. J.; Jones, K. M.; Machol, J. L.; Nozik, A. J. *J. Phys. Chem.* **1995**, *99*, 7754.

(23) Murray, C. B.; Norris, D. J.; Bawendi, M. G. *J. Am. Chem. Soc.* **1993**, *115*, 8706.

(24) Mićić, O. I.; Jones, K. M.; Cahill, A.; Nozik, A. J. *J. Phys. Chem. B.* **1998**, *102*, 9791.

(25) Guzelian, A. A.; Katari, J. E. B.; Kadavanich, A. V.; Banin, U.; Hamad, K.; Juban, E.; Alivisatos, A. P.; Wolters, R. H.; Arnold, C. C.; Heath, J. R. *J. Phys. Chem.* **1996**, *100*, 7212.

(26) Gu, Y.; Lin, Z.; Smetkowski, V.; Butera, R.; Waldeck, D. H. *Langmuir* **1995**, *11*, 1849.

(27) Makky, W. H. In *Properties of Indium Phosphide*; EMIS, Datareviews Series; 1991; p 287.

(28) Becke, A. D. *Phys. Rev. A* **1988**, *38*, 3098.

(29) Lee, C.; Yang, W.; Parr, R. G. *Phys. Rev. B* **1988**, *37*, 785.

(30) Frisch, M. J.; Trucks, G. W.; Schlegel, H. B.; Scuseria, G. E.; Robb, M. A.; Cheeseman, J. R.; Zakrzewski, V. G.; Montgomery, J. A.; Stratmann, R. E.; Burant, J. C.; Dapprich, S.; Millam, J. M.; Daniels, A. D.; Kudin, K. N.; Strain, M. C.; Farkas, O.; Tomasi, J.; Barone, V.; Cossi, M.; Cammi, R.; Mennucci, B.; Pomelli, C.; Adamo, C.; Clifford, S.; Ochterski, J.; Peterson, G. A.; Ayala, P. Y.; Cui, Q.; Morokuma, K.; Malick, D. K.; Rabuck, A. D.; Raghavachari, K.; Foresman, J. B.; Cioslowski, J.; Ortiz, J. V.; Stefanov, B. B.; Liu, G.; Liashenko, A.; Piskorz, P.; Komaromi, I.; Gomperts, R.; Martin, R. L.; Fox, D. J.; Keith, T.; Al-Laham, M. A.; Peng, C. Y.; Nanayakkara, A.; Gonzalez, C.; Challacombe, M.; Gill, P. M. W.; Johnson, B. G.; Chen, W.; Wong, M. W.; Andres, J. L.; Head-Gordon, M.; Replogle, E. S.; Pople, J. A. *Gaussian 98*; Gaussian Inc.: Pittsburgh, PA, 1998.

(31) Ringnalda, M. N.; Langlois, J.; Murphy, R. B.; Greeley, B. H.; Cortis, C.; Russo, T.; Marten, B.; Donnelly, R.; Pollard, W.; Cao, Y.; Muller, R.; Mainz, D.; Wright, J.; Miller, G. H.; III, W. A. G.; Friesner, R. *PS-GVB/Jaguar v. 3.0*; Schrodinger Inc., 1997.

(32) Stewart, J. J. P. *MOPAC 93*; Fujitsu Limited: Tokyo, Japan, 1993.

(33) Calzaferri, G.; Rytz, R.; Brandle, M.; Bruhwiler, D.; Glaus, S. *ICONC*; University of Berne: Berne, Switzerland, 1998.

(34) Hoffmann, R. *Solids and Surfaces*; VCH Publishers: New York, 1988.

(35) *Density Functional Theory of Molecules, Clusters, and Solids*; Ellis, D. E., Ed.; Kluwer Academic Publishers: London, 1995.

(36) Levine, I. N. *Quantum Chemistry*; Prentice Hall: New York, 1991.

(37) Brus, L. E. *J. Chem. Phys.* **1986**, *90*, 2555.